Contemporary Mathematics

A Two-mesh Superconvergence Method for Mesh Adaptivity

Bjørn–Ove Heimsund and Xue-Cheng Tai

Abstract. A two-mesh superconvergent gradient recovery mechanism for elliptic equations is presented. The method first computes the gradient over a fine mesh and then project it to a coarser mesh. This projected gradient has superconvergence properties for general unstructured meshes. The difference between the computed and projected gradient is used as the error indicator in refining a mesh adaptively. This new superconvergence mesh refinement technique is easy to implement and can be used for a large class of problems. Numerical experiments for smooth and singular elliptic problems given in this work show the efficiency of this technique. Comparisons with a classical mesh adaptivity method is also given here to show the advantages.

1. Introduction

In recent years, adaptive algorithms for finite element approximation have been extensively investigated. When producing the mesh, different indicators could be used to refine it [4, 5, 7, 12, 14, 15, 18, 25, 29, 32]. One of the popular indicators is the superconvergence indicator. The well-known ZZ [32] method has been intensively tested and studied for different kind of applications. Recently, we have extended the original ZZ method to a method called MZZ (modified ZZ) method [13]. For the MZZ method, it normally works with two meshes. One is called the "master" mesh which is coarser and one is called the "slave" mesh which is produced by refining the "master" mesh. The finite element solution is computed on the finer slave mesh. After the computation of the finite element solution, we project the gradient or the solution itself to a finite element space of equal or higher order on the master coarser mesh. It is proved that such a procedure gives a solution having superconvergence properties [26, 27]. Contrary to many other superconvergence methods, this procedure does not need to impose uniformity or geometrical symmetry on the mesh. Thus, we use such an indicator to do mesh refinement, and we do not need to impose any conditions on how to refine the mesh. Compared with other adaptive mesh methods [1–6, 8–10, 14, 18–24, 28–31], our method is easy to implement and can be used for a large class of problems.

2. The two-mesh superconvergence method

The method can be used for different kind of applications. We shall consider the model problem:

$$\sum_{i,j=1}^{d} \partial_j(a_{ij}\partial_i u) + \sum_{i=1}^{d} b_i\partial_i u + cu = f \qquad \text{in } \Omega \subset R^d, \tag{2.1}$$

where $\boldsymbol{a} = (a_{ij})_{i,j=1}^d$ is the coefficient tensor which is symmetric, bounded, and uniformly positive definite in a polygonal domain $\Omega \subset R^d$ with measurable entries $a_{ij} = a_{ij}(x)$. The other coefficients $\boldsymbol{b} = (b_i(x))_{i=1}^d$ and $c = c(x)$ are assumed to ensure a uniqueness of solutions for (2.1) such that $u \in H^1(\Omega)$ and $u = g$ on $\partial\Omega$. The method is also correct for other kind of boundary conditions.

Let

$$a(u,v) = \sum_{i,j=1}^{d} \int_\Omega a_{ij}\partial_i u \partial_j v\, dx + \sum_{i=1}^{d} \int_\Omega b_i\partial_i uv\, dx + \int_\Omega cuv\, dx$$

be a bilinear form defined in $H^1(\Omega) \times H^1(\Omega)$. A weak form for the problem (2.1) seeks a function $u \in H^1(\Omega)$ such that $u = g$ on $\partial\Omega$ and

$$a(u,v) = (f,v) \quad \forall v \in H_0^1(\Omega). \tag{2.2}$$

Here we have assumed that the boundary data $g \in H^{1/2}(\partial\Omega)$.

As we have mentioned, we need two meshes for our superconvergence method. We denote T_τ the coarser master finite element partition of Ω. This partition will be used for the post-processing process. The slave finer mesh T_h is always produced by refining the coarser mesh T_τ. This mesh will be used to solve the finite element solution. Corresponding to the two meshes, we also need to two finite element spaces S_h and $\mathcal{L}_\tau$. The space S_h is a scalar finite element space of piecewise polynomials of a given order $k \geq 1$ over the partition T_h. The space $\mathcal{L}_\tau$ is a vector finite element space of piecewise polynomials of order $r \geq 0$ over the partition T_τ. Normally, $\mathcal{L}_\tau$ has higher order, i.e. $r \geq k$. For problem (2.1), we shall require that $S_h \subset H^1(\Omega)$. The finite element solution of (2.2) is a function $u_h = u_h(x)$ in the space $S_h \subset H^1(\Omega)$ such that $u_h(x) = g_h(x)$ for all $x \in \partial\Omega$ and

$$a(u_h,v) = (f,v) \quad \forall v \in S_h^0. \tag{2.3}$$

Here $S_h^0 = H_0^1(\Omega) \cap S_h$ and g_h is a certain approximation of the Dirichlet boundary data g.

The project space $\mathcal{L}_\tau$ can be continuous or discontinuous. Our numerical experiments indicate that the computational cost associated with continuous projection spaces is rather cheap and the recovered solution is normally better than discontinuous projection spaces. Assume that $\mathcal{L}_\tau \subset C^\alpha(\Omega)$. Our analysis [13] indicates that bigger α will give better accuracy for the recovered solution. However, it is not practical to construct finite elements space with $\alpha \geq 1$. Normally, we have $\alpha = 0$.

Once the finite element solution is obtained, we shall do a L^2 projection for the flux $\boldsymbol{q}_h = a\nabla u_h$ to $\mathcal{L}_\tau$. The projected flux $\boldsymbol{Q}_\tau \boldsymbol{q}_h \in \mathcal{L}_\tau$ is the solution of

$$\left(a^{-1}\boldsymbol{Q}_\tau \boldsymbol{q}_h, \phi\right) = (\nabla u_h, \phi)\,, \quad \forall \boldsymbol{\phi} \in \mathcal{L}_\tau. \tag{2.4}$$

Let $\boldsymbol{q} = a\nabla u$. Under some conditions, the projected flux has superconvergence. In order to get superconvergence, we need to assume that there is a fixed real number $1 < s \leq k+1$. The dual problem and the projection finite element space should have some properties. First, the dual problem of (2.2) has H^s-regularity in the sense that for any given $f \in H^{s-2}(\Omega)$, the following problem

$$a(v,w) = (f,v) \quad \forall v \in H_0^1(\Omega)$$

has a unique solution $w \in H_0^1(\Omega) \cap H^s(\Omega)$ such that

$$\|w\|_s + \left\| \frac{\partial w}{\partial \boldsymbol{n}_{\boldsymbol{a}}} \right\|_{s-\frac{3}{2},\partial\Omega} \leq C\|f\|_{s-2}, \tag{2.5}$$

where $\boldsymbol{n}$ is the unit outward normal vector of $\partial\Omega$ and $\frac{\partial w}{\partial \boldsymbol{n}_{\boldsymbol{a}}} = (\boldsymbol{a}\nabla w)\cdot \boldsymbol{n}$ denotes the normal component of the flux variable on the boundary $\partial\Omega$ for the dual solution w. Second, the projection space $\mathcal{L}_\tau$ need to have the following regularity

$$\mathcal{L}_\tau \subset [H^{s-1}(\Omega)]^d. \tag{2.6}$$

Under those conditions, it can be proved that the projected flux has the following superconvergence property [13]:

$$\|\boldsymbol{q} - \boldsymbol{Q}_\tau \boldsymbol{q}_h\|_0 \leq C\tau^{r+1}\|\boldsymbol{q}\|_{r+1,\tau} + C(h\tau^{-1})^{s-1}\|u-u_h\|_1. \tag{2.7}$$

Since $s > 1$, $h\tau^{-1} \ll 1$, we have $\|\boldsymbol{q} - \boldsymbol{Q}_\tau\boldsymbol{q}_h\|_0 \ll \|u-u_h\|_1$ if we choose the polynomial order r sufficiently high and the mesh size τ sufficiently coarse. Accordingly, we have

$$\|\boldsymbol{Q}_\tau q_h - q_h\|_0 \cong \|q - q_h\|_0,$$

which means that we could use $\|\boldsymbol{Q}_\tau q_h - q_h\|$ as an indicator to do mesh refinement.

2.1. Mesh adaptivity. In our computations, only the coarse mesh T_τ will be produced adaptively. The fine mesh T_h is always a refinement of T_τ. We also take S_h and $\mathcal{L}_\tau$ to be linear finite element spaces over T_h and T_τ respectively. Each element of T_τ is refined into four equal elements to get the mesh T_h. Thus, we only need to store the information of mesh T_τ in the computer, the mesh T_h is known from the mesh structure of T_τ.

For a given tolerance ϵ, we want to adaptively produce the meshes such that

$$\|\boldsymbol{Q}_\tau\boldsymbol{q}_h - \boldsymbol{q}_h\| \leq \epsilon. \tag{2.8}$$

To this end, for a given coarse mesh $\mathcal{L}_\tau$, we compute the maximum value of the left hand side of Equation (2.8) over all the coarse mesh elements:

$$\eta_\tau = \max_{K\in T_\tau} \|\boldsymbol{Q}_\tau\boldsymbol{q}_h - \boldsymbol{q}_h\|_{0,K}.$$

We choose a parameter $\theta \in (0,1)$. For a given coarse mesh element $K \in T_\tau$, we refine K if

$$\|\boldsymbol{Q}_\tau\boldsymbol{q}_h - \boldsymbol{q}_h\|_{0,K} \geq \theta\eta_\tau.$$

The refinement process is stopped if either (2.8) is satisfied, the memory limit has been reached, or the change of the computed solution in the energy norm is less than a given tolerance. More formally, this indicator function will be refered to as

$$E_G(K) = \|\boldsymbol{Q}_\tau\boldsymbol{q}_h - \boldsymbol{q}_h\|_{0,K}\,,$$

meaning that the element $K \in T_\tau$ is refined if

$$E_G(K) \geq \theta \max_{e\in T_\tau} E_G(e).$$

In order to show the efficiency of our error indicator, we shall compare the mesh produced by our method with the jump error indicator of [12, 16]. The error indicator of [12, 16] is based on the homogeneous Dirichlet problem for

$$\Delta u = f,$$

where one can show that a computed finite element solution of the flux $\boldsymbol{q}_h$ satisfied the error estimate

$$\|\boldsymbol{q}_h - \boldsymbol{q}\|_{0,K} \le \alpha \|hf\|_K + \beta \sqrt{\sum_{\Gamma_i \in \partial K} |\Gamma_i|^2 \left[\frac{\partial u_h}{\partial \boldsymbol{n}_{\Gamma_i}}\right]^2},$$

where $[\cdot]$ is the jump on the edge Γ_i of $K \in \Omega_h$ and α and β are mesh independent constants. When the conductivity is non-constant, and we solve for

$$\nabla \cdot (a \nabla u) = f,$$

the error indicator

$$E_J(K) = \alpha \|hf\|_K + \beta \sqrt{\sum_{\Gamma_i \in \partial K} |\Gamma_i|^2 \left[\boldsymbol{n}_{\Gamma_i} \cdot \boldsymbol{q}_h\right]^2} \tag{2.9}$$

is used instead. This method does not need to work on two meshes simultaneously. As earlier, an element $K \in \Omega_h$ is then refined if

$$E_J(K) \ge \theta \max_{e \in T_h} E_J(e).$$

In the numerical experiments, the indicators $E_G(K)$ and $E_J(K)$ will be compared.

3. Numerical results

To illustrate the performance of our flux recovery method and its use in mesh adaption, we will compare our indicator $E_G(K)$ with the standard mesh adaption technique of [12, 16] given by $E_J(K)$. Comparisons with other recovery schemes has been provided in [13] and will not be repeated here.

The function value errors are computed by

$$\|u_h - u\|_0 = \sqrt{\sum_{K \in T_h} \int_K (u_h - u)^2 \, dx\, dy}. \tag{3.1}$$

and the gradient error is computed by

$$\|\nabla u_h - \nabla u\|_0 = \sqrt{\sum_{K \in T_h} \int_K \left[((u_h)_x - u_x)^2 + ((u_h)_y - u_y)^2\right] dx\, dy}. \tag{3.2}$$

The integration over each element is computed by a sixth order quadrature rule. Furthermore, we set $\alpha = \beta = 0.15$ in Equation (2.9). The tolerance θ is chosen experimentally on a case by case basis to ensure a smooth refinement, typically $\theta = 0.4$.

In the error-plots, we always use logarithmic axis in which the x-axis is the degrees of freedom (DoF) of the triangulation, while the y-axis is either the function error or the gradient error. A solid line will denote the error computed on the mesh produced by E_G, dashed line is for the error by E_J and the dashed-dotted line is for the error of the recovered gradient $Q_\tau q_h$.

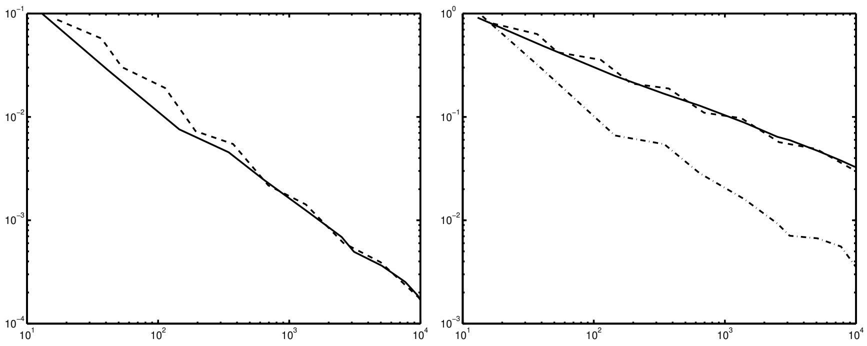

(a) Function error (3.1) (b) Gradient error (3.2)

FIGURE 1. Error plots for the smooth problem in §3.1, The rate of convergence of the recovered gradient using E_G is 0.85, while the rate is 0.53 using E_G.

We shall also measure the rate of convergence of the gradients. The convergence rate is evaluated using the following formula:

$$\text{order} = -\frac{\log_{10}\text{error}(k) - \log_{10}\text{error}(0)}{\log_{10}\text{DoF}(k) - \log_{10}\text{DoF}(0)}, \tag{3.3}$$

in which error(0) is the first computational gradient error, while error(k) is the last. DoF(0) and DoF(k) are the corresponding degrees of freedoms.

3.1. Smooth problem. As a reference case, we will show the performance of the indicators applied to the smooth problem

$$-\Delta u = 2\pi^2 \sin(\pi x)\sin(\pi y), \quad \text{in } \Omega = (0,1)\times(0,1),$$

with zero Dirichlet boundary conditions. The solution to this problem is obviously

$$u = \sin(\pi x)\sin(\pi y).$$

The functional error and gradient errors are shown in Figure 1, and the meshes produced by the two indicator functions are presented in Figure 2. The convergence rate for the recovered gradient using E_G is clearly better than those recovered by E_J, while the functional error is generally smaller for the mesh produced by the E_G indicator.

It is also instructive to investigate the error distribution of the gradients on the different meshes. In Figures 3-4 we have plotted the pointwise error

$$\sqrt{\left(u_x^h - u_x\right)^2 + \left(u_y^h - u_y\right)^2}$$

in which u_x^h and u_y^h are the computed solution derivatives. From the figure, it is clear that the recovered gradient on the mesh produced by the E_G indicator is overall smaller, while the E_J mesh has a gradient with larger errors near the four corners.

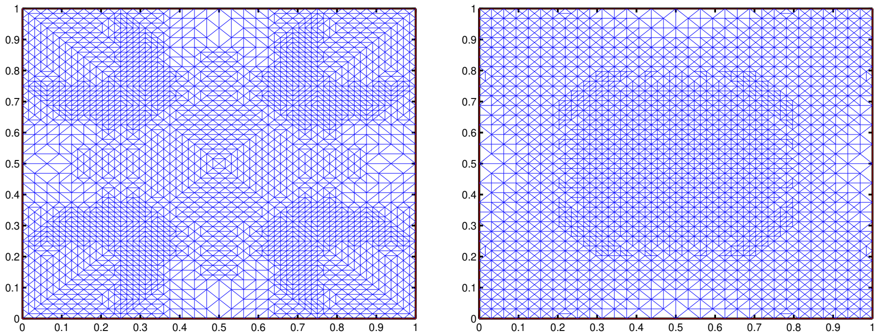

(a) Mesh produced by E_G

(b) Mesh produced by E_J

FIGURE 2. Meshes for the smooth problem of §3.1. The left mesh has 2513 nodes and a gradient error of $9.309 \cdot 10^{-3}$, while the right has 2589 nodes with a gradient error of $5.7 \cdot 10^{-2}$

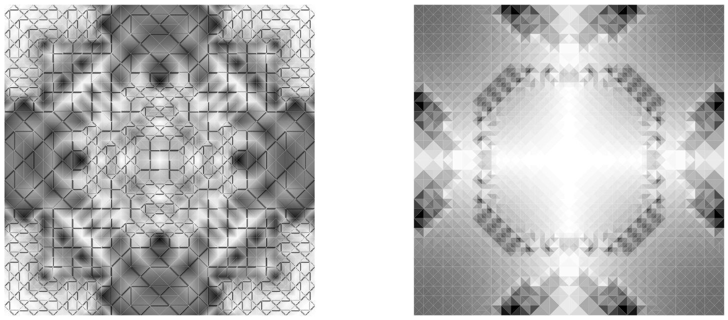

(a) E_G gradient error distribution

(b) E_J gradient error distribution

FIGURE 3. The distribution of the gradient errors on some coarser meshes produced by the two indicators for the smooth problem of §3.1. The E_G mesh has 1153 nodes with largest pointwise error of 0.060982, while the E_J mesh has 1337 nodes and largest error of 0.144607. Dark areas have large errors, while light areas have small errors.

3.2. Discontinuous coefficients. A problem which has a singularity due to a discontinuous conductivity coefficient is

$$-\nabla \cdot (\boldsymbol{a}(x, y)\nabla u) = 0, \quad \text{in } \Omega = (0, 1) \times (0, 1), \tag{3.4}$$

where $\boldsymbol{a}(x, y)$ is scalar-valued and equal 1 in the first and third quadrants, and equal R in the other two quadrants. The solution in polar coordinates is $u(r, \theta) = r^\gamma \mu(\theta)$,

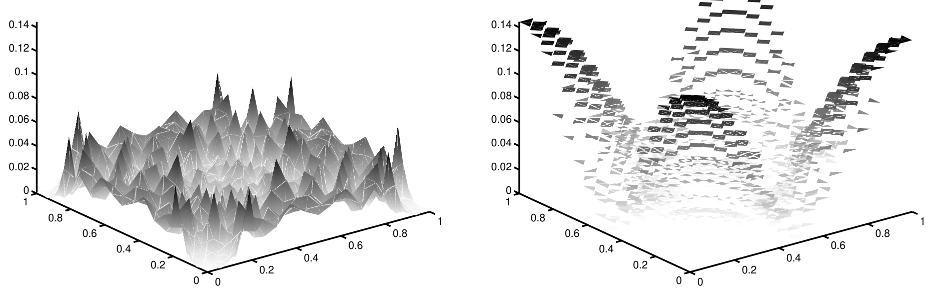

(a) E_G gradient error distribution (b) E_J gradient error distribution

FIGURE 4. 3D plot of the same data as in Figure 3. Note that the recovered gradient is piecewise linear and globally continuous, while the gradient produced by the linear finite element method is piecewise constant.

and is due to [17]. It is

$$\mu(\theta) = \begin{cases} \cos\left(\left(\frac{\pi}{2}-\sigma\right)\gamma\right)\cos\left(\left(\theta-\frac{\pi}{2}+\rho\right)\gamma\right), & 0 \le \theta < \frac{\pi}{2} \\ \cos(\rho\gamma)\cos\left((\theta-\pi+\sigma)\gamma\right), & \frac{\pi}{2} \le \theta < \pi \\ \cos(\sigma\gamma)\cos\left((\theta-\pi-\rho)\gamma\right), & \pi \le \theta < \frac{3\pi}{2} \\ \cos\left(\left(\frac{\pi}{2}-\rho\right)\gamma\right)\cos\left(\left(\theta-\frac{3\pi}{2}-\sigma\right)\gamma\right), & \frac{3\pi}{2} \le \theta < 2\pi \end{cases}$$

in which the numbers γ, ρ, σ and R satisfy the conditions

$$\begin{aligned} R &= -\tan\left(\left(\tfrac{\pi}{2}-\sigma\right)\gamma\right)\cot(\rho\gamma), \\ \tfrac{1}{R} &= -\tan(\rho\gamma)\cot(\sigma\gamma), \\ R &= -\tan(\sigma\gamma)\cot\left(\left(\tfrac{\pi}{2}-\rho\right)\gamma\right), \end{aligned} \tag{3.5}$$

along with the inequalities

$$\begin{array}{rcccl} 0 & < & \gamma & < & 2, \\ \max(0, \pi\gamma-\pi) & < & 2\gamma\rho & < & \min(\pi\gamma, \pi), \\ \max(0, \pi-\pi\gamma) & < & -2\gamma\rho & < & \min(\pi, 2\pi-\pi\gamma). \end{array} \tag{3.6}$$

For a given value of γ, Equations (3.5)-(3.6) can be solved for γ, ρ and σ, and in [17] several solutions were provided where $\rho = \pi/4$. Here we will consider

$$\begin{aligned} \gamma &= 0.5, \\ R &\approx 5.8284271247461907, \\ \sigma &\approx -2.3561944901923448. \end{aligned} \tag{3.7}$$

Adaptive finite element methods for this problem has been studied [7, 25], however their goal was reducing the error $\|u_h - u\|_0$ and not necessarily the error in the gradient. Applying the two indicator functions to this problem gives the computational results in Figure 5 along with the produced meshes in Figure 6. We see that the function errors are steadily decreased, while the reduction of the gradient

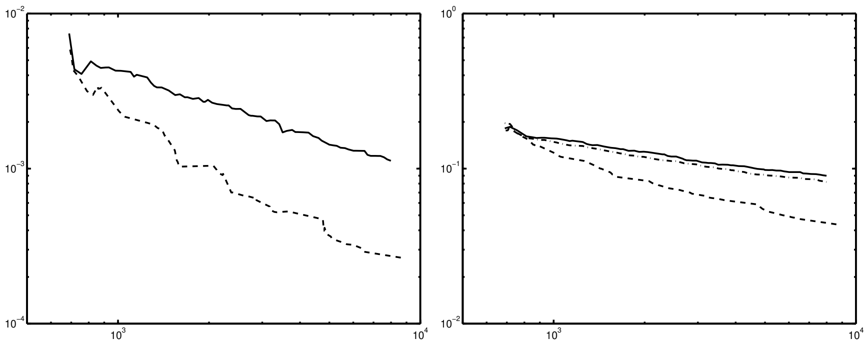

(a) Function error (3.1)   (b) Gradient error (3.2)

Figure 5. Plots of the errors (3.2) for the problem in §3.2 with $\gamma = 0.5$. The convergence rate for the gradients is slower here, and it is clear that the E_J indicator does a rather better job than the E_G indicator. The rate of convergence of the E_J indicator is 0.55, while E_G has a convergence rate of 0.36.

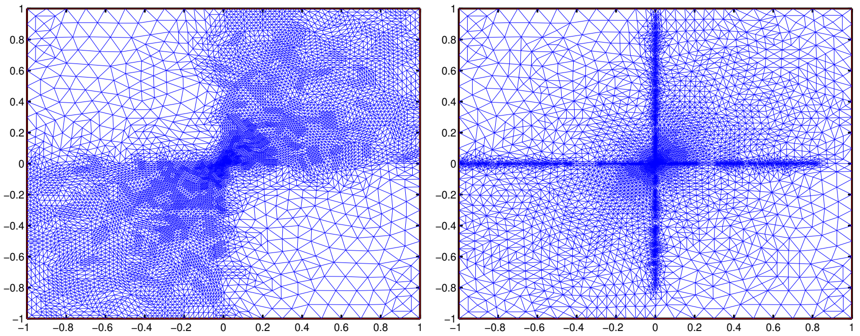

(a) Mesh produced by E_G (b) Mesh produced by E_J

Figure 6. Meshes produced by the E_G and E_J error indicators used on the problem in §3.2 with $\gamma = 0.5$. The meshes for the other values of γ do not differ much. The E_G mesh is with 7993 nodes and a gradient error of $8.196 \cdot 10^{-2}$ after the gradient recovery has been applied. The indicator E_J produced a mesh with 8715 degrees of freedom and a gradient error of $4.325 \cdot 10^{-2}$.

error is slower. Also, the classical indicator E_J consistently outperforms the E_G indicator, even for the gradient.

Figure 7 shows the gradient error distributions as was shown for the smooth problem in § 3.1. While the E_J indicator has a small error in large portions of the

(a) E_G gradient error distribution (b) E_J gradient error distribution

FIGURE 7. Gradient error distribution plot for the discontinuous coefficient problem of §3.2. The left mesh has 909 nodes with maximum error of 2.105516 and the right mesh has 826 nodes and a max error equal 4.148048.

domain, however it has a larger error at origin. As the mesh is further refined, the error in the origin is dominating.

3.3. Corner singularity. The next problem has a singularity induced by a reentrant corner, and is

$$\begin{aligned} \Delta u &= 0, \quad && \text{in } \Omega, \\ u &= u_0, \quad && \text{on } \partial\Omega, \end{aligned}$$

in which

$$\Omega = \left\{ (r,\theta) : 0 < r < 1, 0 < \theta < \frac{\pi}{\gamma} \leq 2\pi \right\}.$$

The exact solution is $u(r,\theta) = r^\gamma \sin(\gamma\theta)$ and the boundary data u_0 is taken to be consistent with the analytical solution. It is easy to see that the regularity of the solution depends directly on γ. We will consider the case with $\gamma = 4/3$ and $\gamma = 2/3$, $u \in H^2$ for the former choice, but not for the latter.

The meshes produced for the case of $\gamma = 4/3$ are shown in Figure 9, and plots of the error (3.2) are in Figure 8. This can be compared with the case of $\gamma = 2/3$ given in Figures 10-11. In both cases we see that the recovered gradient is clearly superconvergent, while the function errors comparing the two meshes are comparable to one another.

We note that this particular corner singularity problem has been studied earlier in [11] where an indicator function based on the jumps of the gradient across the edges of each element was used. The tests here show clearly that our method can handle this problem better than the E_J indicator, especially with regards to the accuracy of the recovered gradient.

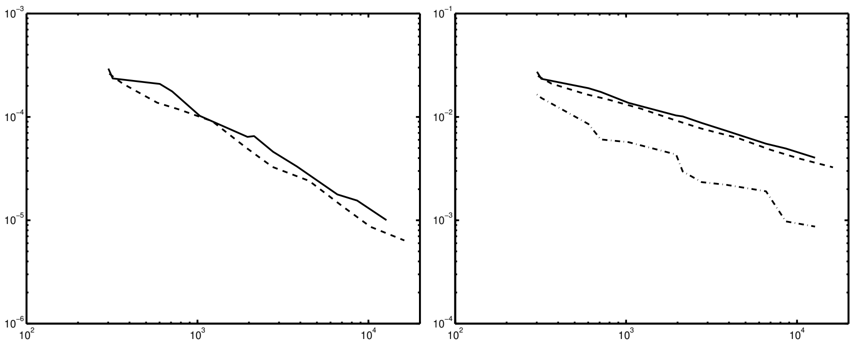

(a) Function error (3.1) (b) Gradient error (3.2)

FIGURE 8. Plots of the errors for the corner singularity problem in §3.3 with $\gamma = 4/3$, giving the meshes in Figure 9. The rate of convergence of the recovered gradient is 0.84, while the rate of convergence of the gradient produced by the standard adaption is 0.51.

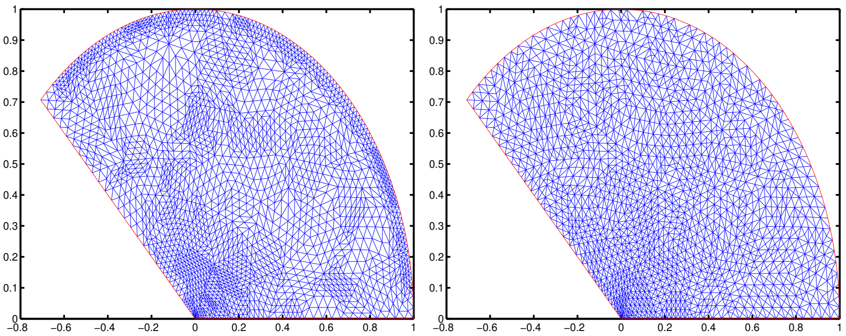

(a) Mesh produced by E_G (b) Mesh produced by E_J

FIGURE 9. Meshes produced by the mesh adaptivity schemes applied to the corner singularity problem of §3.3 with $\gamma = 4/3$. The mesh given by E_G is shown with 2144 nodes and has a recovered gradient error of $2.967 \cdot 10^{-3}$ while the mesh produced with E_J is with 1925 nodes and an error of $9.313 \cdot 10^{-3}$.

3.4. Mixed Dirichlet/Neumann problem. The last problem we shall consider is the mixed Dirichlet/Neumann problem, also studied in [11]. It is

$$\begin{aligned} \Delta u &= 0, && \text{in } \Omega, \\ \frac{\partial u}{\partial n} &= 0, && \text{on } \Gamma_1, \\ u &= u_0, && \text{on } \Gamma_2, \end{aligned}$$

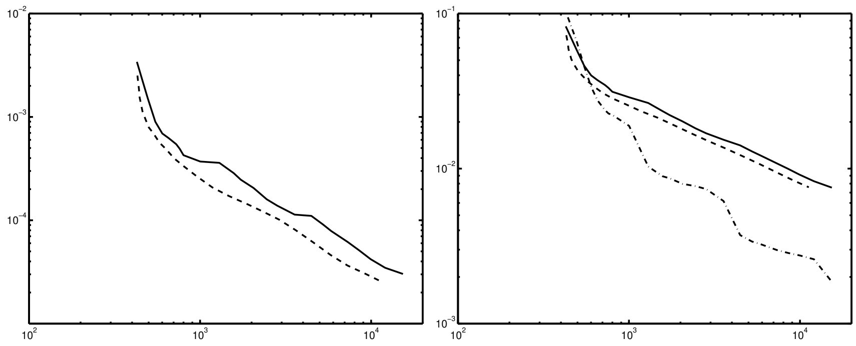

(a) Function error (3.1) (b) Gradient error (3.2)

FIGURE 10. Plots of the errors for the corner singularity problem in §3.3 with $\gamma = 4/3$, with the associated meshes of Figure 11. Here the convergence rate of the recovered gradient using E_G is 1.12, and it has a rate of 0.69 for the E_J indicator.

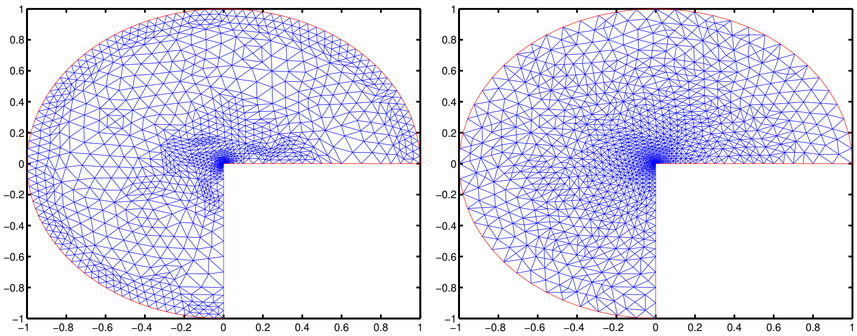

(a) Mesh produced by E_G (b) Mesh produced by E_J

FIGURE 11. Meshes produced by the mesh adaptivity schemes applied to the corner singularity problem of §3.3 with $\gamma = 2/3$. Left mesh has 1297 nodes with a recovered gradient error of $1.03 \cdot 10^{-2}$ and the right has 1473 nodes and a gradient error of $2.127 \cdot 10^{-2}$.

where

$$\begin{aligned}
\Omega &= \{(r,\theta) : 0 < r < 1, 0 < \theta < \pi\}, \\
\Gamma_1 &= \{(r,\theta) : 0 < r \leq 1, \theta = \pi\}, \\
\Gamma_2 &= \partial\Omega \setminus \Gamma_1.
\end{aligned}$$

The analytical solution is $u(r,\theta) = \sqrt{r}\sin\left(\frac{\theta}{2}\right)$ and the Dirichlet boundary data is chosen consistent with this solution. Note that ∇u is singular as $|x|, |y| \to 0$.

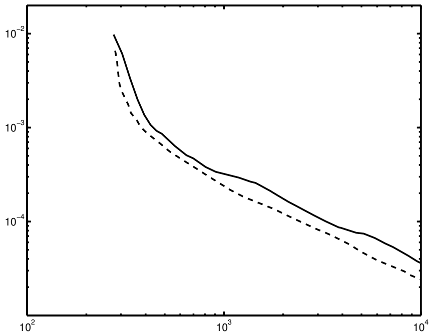

(a) Function error (3.1)

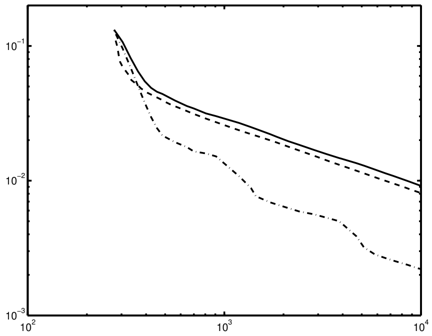

(b) Gradient error (3.2)

FIGURE 12. Plots of the errors for the mixed Dirichlet/Neumann problem in §3.4. The rate of convergence for the recovered gradient for E_G is 1.12, while E_J indicator has a rate of 0.72.

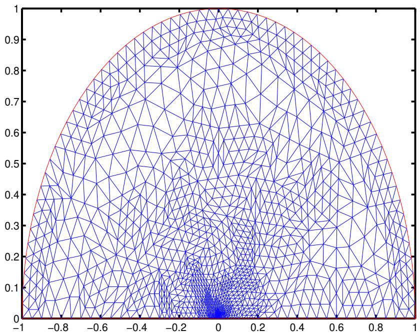

(a) Mesh produced by E_G

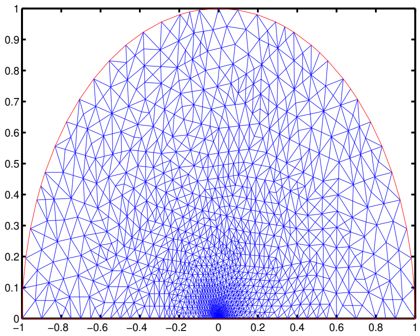

(b) Mesh produced by E_J

FIGURE 13. Meshes produced by the different mesh adaptivity schemes applied to the mixed Dirichlet/Neumann problem of §3.4. The mesh for the E_G indicator is shown with 1447 nodes and a projected gradient error of $7.671 \cdot 10^{-3}$ while the E_J produced mesh has 1565 degrees of freedom and a gradient error of $2.078 \cdot 10^{-2}$.

Error-plots are given in Figure 12 followed by the corresponding meshes in Figure 13. Again, note the superconvergence behaviour of the recovered gradient. This time around, the E_J indicator produces the smallest functional error, but the recovered gradient given by E_G is an order of magnitude more accurate than the regular gradient.

4. Concluding remarks

Mesh adaptivity has been widely studied in the literature. We have proposed a two-mesh superconvergence method which provides both a much more accurate gradient than classical methods, and offers an associated mesh refinement indicator.

The advantages of this scheme is that it can be easily used for a wide range of problems. The implementation for different kind of problems is easier than other approaches. Our numerical experiments show that the method works well for smooth problems as well as for problems with singularities.

References

1. Roland Becker and Rolf Rannacher, *An optimal control approach to a posteriori error estimation in finite element methods*, Acta Numer. **10** (2001), 1–102. MR **MR2009692 (2004g:**65147)
2. Carsten Carstensen, *Some remarks on the history and future of averaging techniques in a posteriori finite element error analysis*, ZAMM Z. Angew. Math. Mech. **84** (2004), no. 1, 3–21. MR MR2031241
3. Carsten Carstensen and Georg Dolzmann, *An a priori error estimate for finite element discretizations in nonlinear elasticity for polyconvex materials under small loads*, Numer. Math. **97** (2004), no. 1, 67–80. MR MR2045459
4. Carsten Carstensen and R. Klose, *A posteriori finite element error control for the p-Laplace problem*, SIAM J. Sci. Comput. **25** (2003), no. 3, 792–814 (electronic). MR MR2046112
5. Carsten Carstensen and Stefan A. Sauter, *A posteriori error analysis for elliptic PDEs on domains with complicated structures*, Numer. Math. **96** (2004), no. 4, 691–721. MR **MR2036362 (2004k:**65212)
6. Zhiming Chen and Shibin Dai, *Adaptive Galerkin methods with error control for a dynamical Ginzburg-Landau model in superconductivity*, SIAM J. Numer. Anal. **38** (2001), no. 6, 1961–1985 (electronic). MR **MR1856238 (2002g:**65114)
7. Zhiming Chen and Shibin Dai, *On the efficiency of adaptive finite element methods for elliptic problems with discontinuous coefficients*, SIAM Journal of Scientific Computing **24** (2002), no. 2, 443–462.
8. Zhiming Chen and Jia Feng, *An adaptive finite element algorithm with reliable and efficient error control for linear parabolic problems*, Math. Comp. **73** (2004), no. 247, 1167–1193 (electronic). MR MR2047083
9. Zhiming Chen and Ricardo H. Nochetto, *Residual type a posteriori error estimates for elliptic obstacle problems*, Numer. Math. **84** (2000), no. 4, 527–548. MR **MR1742264 (2001c:**65134)
10. Liu Du and Ningning Yan, *Gradient recovery type a posteriori error estimate for finite element approximation on non-uniform meshes*, Adv. Comput. Math. **14** (2001), no. 2, 175–193. MR **MR1843305 (2002h:**65180)
11. Kenneth Eriksson and Claes Johnson, *An adaptive finite element method for linear elliptic problems*, Mathematics of Computation **50** (1988), no. 182, 361–383.
12. ______, *Adaptive finite element methods for parabolic problems I: A linear model problem*, SIAM Journal of Numerical Analysis **28** (1991), 43–77.
13. Bjørn-Ove Heimsund, Xue-Cheng Tai, and Junping Wang, *Superconvergence for the gradient of finite element approximations by L^2 projections*, SIAM Journal of Numerical Analysis **40** (2002), no. 4, 1263–1280.
14. V. Heuveline and R. Rannacher, *Duality-based adaptivity in the hp-finite element method*, J. Numer. Math. **11** (2003), no. 2, 95–113. MR MR1987590
15. W. Hoffmann, A. H. Schatz, L. B. Wahlbin, and G. Wittum, *Asymptotically exact a posteriori estimators for the pointwise gradient error on each element in irregular meshes*, Math. Comp. **70** (2001), 897–909.
16. Claes Johnson, *Numerical solution of partial differential equations by the finite element method*, Cambridge university press, 1987.
17. R. B. Kellogg, *On the Poisson equation with intersecting interface*, Appl. Anal. **4** (1975), 101–129.

18. Ruo Li, Tao Tang, and Pingwen Zhang, *Moving mesh methods in multiple dimensions based on harmonic maps*, J. Comput. Phys. **170** (2001), no. 2, 562–588. MR **MR1844903 (2002e:**65139)
19. ———, *A moving mesh finite element algorithm for singular problems in two and three space dimensions*, J. Comput. Phys. **177** (2002), no. 2, 365–393. MR **MR1897293 (2003c:**65093)
20. Wenbin Liu and Ningning Yan, *Quasi-norm a priori and a posteriori error estimates for the nonconforming approximation of p-Laplacian*, Numer. Math. **89** (2001), no. 2, 341–378. MR **MR1855829 (2002g:**65136)
21. ———, *Quasi-norm local error estimators for p-Laplacian*, SIAM J. Numer. Anal. **39** (2001), no. 1, 100–127 (electronic). MR **MR1860718 (2002i:**65131)
22. ———, *Some a posteriori error estimators for p-Laplacian based on residual estimation or gradient recovery*, J. Sci. Comput. **16** (2001), no. 4, 435–477 (2002). MR **MR1881854 (2002k:**65191)
23. ———, *On quasi-norm interpolation error estimation and a posteriori error estimates for p-Laplacian*, SIAM J. Numer. Anal. **40** (2002), no. 5, 1870–1895 (electronic). MR **MR1950626 (2003m:**65207)
24. ———, *A posteriori error estimates for optimal control problems governed by parabolic equations*, Numer. Math. **93** (2003), no. 3, 497–521. MR **MR1953750 (2003k:**49067)
25. P. Morin, R. H. Nochetto, and K. G. Siebert, *Data oscillation and convergence of adaptive FEM*, SIAM Journal of Numerical Analysis **38** (2000), 466–488.
26. J. Wang, *A superconvergence analysis for finite element solutions by the least-squares surface fitting on irregular meshes for smooth problems*, Journal of Mathematical Study **33** (2000), no. 3, 229–243.
27. J. Wang and X. Ye, *Superconvergence of finite element approximations for the Stokes problem by projection methods*, SIAM J. Numer. Anal. **39** (2001), 1001–1013.
28. Ningning Yan, *A posteriori error estimators of gradient recovery type for elliptic obstacle problems*, Adv. Comput. Math. **15** (2001), no. 1-4, 333–362 (2002), A posteriori error estimation and adaptive computational methods. MR **MR1887739 (2003a:**65090)
29. Ningning Yan and Aihui Zhou, *Gradient recovery type a posteriori error estimates for finite element approximations on irregular meshes*, Comput. Methods Appl. Mech. Engrg. **190** (2001), no. 32-33, 4289–4299. MR **MR1832657 (2002c:**65189)
30. Zhimin Zhang, *Polynomial preserving gradient recovery and a posteriori estimate for bilinear element on irregular quadrilaterals*, Int. J. Numer. Anal. Model. **1** (2004), no. 1, 1–24. MR MR2052728
31. Aihui Zhou (ed.), *A posteriori error estimation and adaptive computational methods*, Kluwer Academic Publishers, Dordrecht, 2002, Adv. Comput. Math. **15** (2001), no. 1-4. MR MR1887726
32. O. C. Zienkiewicz and J. Z. Zhu, *The superconvergent patch recovery and a posteriori error estimates, parts 1 and 2*, Intert. J. Numer. Methods Engrg. (1992), 1331–1364 and 1365–1382.

Centre of Integrated Petroleum Research, University of Bergen, Norway
E-mail address: `Bjorn-Ove.Heimsund@uib.no`

Department of Mathematics, University of Bergen, Norway
E-mail address: `tai@math.uib.no`